Coherent x-ray scattering and dynamics of fluctuations in smectic-*A* and crystal-*B* films: Continuous model

A. N. Shalaginov and D. E. Sullivan
Department of Physics and Guelph-Waterloo Physics Institute, University of Guelph, Guelph, Ontario, Canada N1G 2W1
(Received 7 February 2000)

We present a theoretical study of the dynamic displacement-displacement and intensity-intensity (for coherent soft x-ray scattering) correlations in Sm-*A* as well as Cr-*B* free-standing films. The work is based on a continuous hydrodynamic model that allows one to calculate efficiently the dynamic correlation functions and considerably simplifies earlier analyses of finite-size and surface effects in Sm-*A* films. The model is extended to Cr-*B* films. We show that despite the crystalline order, the Cr-*B* film is a strongly fluctuating system, which is due to an abnormally small shear elastic constant. An easy-shear approximation is developed to describe the fluctuations in the Cr-*B* phase. We predict nonmonotonic behavior of the intensity-intensity correlation function in both Sm-*A* and Cr-*B* films. The analysis can be applied to either coherent x-ray or conventional laser dynamic light scattering experiments.

PACS number(s): 61.30.Cz, 83.70.Jr

I. INTRODUCTION

Although the idea of studying dynamical processes by means of scattering is not new and conventional light scattering has been widely used since lasers became available, coherent x-ray dynamic scattering studies have been carried out only recently. In particular, there have been a number of recent theoretical and experimental dynamical studies of layer fluctuations in free-standing films made of smectic-*A* liquid crystals [1–3]. A smectic liquid crystal consists of a stack of two-dimensional liquid layers. Mean-square thermal undulations of the layers diverge logarithmically with the size of the system due to the Landau-Peierls instability. The number of layers in a film can vary from two to a few thousand, so that the films provide a good opportunity to study crossover from two-dimensional to three-dimensional behavior and surface effects on phase transitions. The first dynamical light-scattering study of free-standing smectic liquid-crystal films was carried out in Ref. [4]. Light-scattering experiments are sensitive either to orientational fluctuations of molecules associated with layer undulations [5,6] or to fluctuations of the air-liquid interface (as in the case of Ref. [4]), but not the undulations themselves. They also do not probe distances of the order of the layer spacing. In contrast, x-ray dynamic scattering experiments are sensitive to the layer undulations and give much better spatial resolution. Nevertheless, their analysis is more difficult than that of light-scattering studies. In the latter case, it is sufficient to calculate the two-time displacement-displacement correlation function in the wave-vector, frequency $(\mathbf{q},\omega)$ representation, while a x-ray dynamic scattering study requires the position, time $(\mathbf{r},t)$ representation, which neccesitates taking the inverse Fourier transform. For both light-scattering and x-ray scattering, finite-size and surface effects require that one take into account surface tension and perhaps other surface parameters. Finite size also leads to quantization, producing a set of modes dependent on surface parameters instead of a continuous spectrum.

The dynamics of smectic-*A* films can be analyzed by hydrodynamic theory using either a set of linear equations (discrete model) or an ordinary differential equation with boundary conditions (continuous model). There have been a number of theoretical studies of single-time correlation functions based on both a discrete model [7,8] and a continuous model [6,9]. Excluding very narrow regions close to interfaces, these models yield the same correlation function. The continuous model was successfully used to fit scattering data [10] and extract the surface tension and elastic constants. It has been shown that the profile of mean-square displacement fluctuations predicted by these models plays a crucial role in layer-by-layer crystallization in free-standing smectic films [11].

The two-time correlation function of thermal displacements of the layers is required for analysis of x-ray dynamic scattering. Recently, this has been examined both by a discrete model [2,3] as well as by a continuous one [12]. Both models are based on the hydrodynamic equations for bulk systems, supplemented by boundary conditions. It has also been argued for both models that, in the relevant time scales, the permeation process is very slow and does not effect dynamics. The boundary conditions used in [12] implicitly assume that relaxation at the interfaces is much faster than in the bulk (i.e., the viscosity at the interfaces is negligible) and represent the balance of elastic forces at the interfaces. In this paper we derive a continuous model based on the same assumptions as in [12], but analyze it by a different mathematical approach that directly yields a closed-form expression for the correlation function in the $(\mathbf{q},\omega)$ representation. The relaxation times of the modes correspond to the poles of this function, which are shown to agree with those derived in Ref. [12]. We also show that the continuous model yields the same characteristic times as the discrete model [2,3], but with a considerably simplified analysis.

Quite unexpected results have been recently obtained for a film in the crystal-*B* phase [13]. One would expect that the crystalline structure produces a large bending rigidity of the film. According to the conventional theory for solid plates [14], undulation of a thin elastic plate gives rise to extension of one side (top or bottom) and compression of the other

side. It has been shown [14] that the bending rigidity in this case is on the order of L^2E, where L is the film thickness and E is Young's modulus. In the case of a Cr-B film, Young's modulus is the ratio of uniaxial in-plane stress to uniaxial in-plane strain in the plates. Estimating the order of magnitude of the bending rigidity using the value of E expected for a hexagonal two-dimensional crystal [15], one finds that the crystal-associated rigidity for a ten-layer film is 10^3 larger than the nematic elastic constant K and hence should drastically affect diffuse x-ray scattering. However, it is found that the rigidity remains the same when a Sm-A film is cooled and becomes a crystalline plate [13]. Therefore, it is of interest to explain this effect theoretically and make predictions for the dynamical behavior of the Cr-B phase. In this paper we extend the continuous dynamical model to the Cr-B phase. We show that the unexpectedly small observed bending rigidity is due to well-developed shear deformations in a Cr-B plate. We also show that inertial terms are crucial for long wavelength fluctuations and in general are not negligible.

The paper is organized as follows. In Sec. II we review the scattering intensity in the first Born approximation and its relation to the displacement-displacement correlation function. In Sec. III the basic hydrodynamics of smectic-A liquid crystals is described and the assumptions underlying the model are stated, followed by development of the model itself. To expose our method clearly, inertial effects are neglected in this section (as done in the analysis of the discrete model in Ref. [2]), recognizing that this neglect may not be valid for very thin Sm-A films. The displacement-displacement correlation function is expressed in terms of the resolution function of the operator $-\nabla_z^2$. This is an alternative to the analysis in Ref. [12], which is based on representing the correlation function as a series in the eigenfunctions of $-\nabla_z^2$. The dependence of characteristic relaxation times on physical parameters of the system is analyzed and shown to agree with earlier results [2,3,12]. In Sec. IV dynamical equations for the Cr-B phase are derived. A simplified approach is developed based on the fact that in this type of crystal the shear elastic constant is abnormally small. A final dynamical equation is written in terms of displacements of the layers, which slide over each other almost freely. The correlation function is derived by analogy with that for the Sm-A phase. It is shown that a finite shear elastic constant removes the small parameter $\rho_0 K/\eta_3^2$ [16] which usually allows one to neglect inertial terms in the case of a Sm-A phase (where ρ_0 is the mass density and η_3 is the layer-normal shear viscosity coefficient [17]). The intensity correlation function is explicitly evaluated in the limit of very thin films where one can neglect the layer compressibility modulus. It is shown that the intensity correlation function exhibits oscillatory behavior at long times due to the inertial terms, a result which also applies to thin Sm-A films. In Sec. V the results are summarized and a short discussion is given. In the Appendix we show how the continuous model can be related to the discrete one.

II. SCATTERED INTENSITY AND THE DISPLACEMENT-DISPLACEMENT CORRELATION FUNCTION

A coherent x-ray beam enables one to measure $\langle I(t)I(0)\rangle$ and obtain information about dynamical processes in the system under consideration. Let us consider in more detail the correlation between intensities $I(t)$ at different times. We recall that the intensity at time t is proportional to $E(t)E^*(t)$, where E is the electric field. The measured correlation function is therefore proportional to $\langle E(0)E^*(0)E(t)E^*(t)\rangle$. If fluctuations of the field are Gaussian, then the intensity-intensity correlation factorizes as

$$\begin{aligned}\langle E(0)E^*(0)E(t)E^*(t)\rangle = &\langle E(0)E(t)\rangle\langle E(0)^*E^*(t)\rangle \\ &+\langle E(0)E^*(0)\rangle\langle E(t)E^*(t)\rangle \\ &+\langle E(0)E^*(t)\rangle\langle E^*(0)E(t)\rangle.\end{aligned} \tag{1}$$

Taking into account that the field changes with time as $e^{\imath\omega t}$, we find that the first term becomes zero after averaging over the period $2\pi/\omega$. The second term does not depend on time, because the system is stationary (i.e., the single-time correlation function does not depend on time). The third term contains all information about the dynamics and is proportional to $|S|^2$, where S in the first Born approximation is given by

$$S=\int d^3r\langle\rho(\mathbf{r},t)\rho(0,0)\rangle e^{\imath\mathbf{r}\cdot\mathbf{q}}, \tag{2}$$

where $\mathbf{q}$ is the scattering vector. In a smectic-A liquid crystal the electron density is

$$\rho(\mathbf{r},t)=\rho_s(z)\sum_n \delta[z-nd-u_n(\mathbf{r}_\perp,t)], \tag{3}$$

where the z axis is taken perpendicular to the layers and the vector $\mathbf{r}$ has components $(\mathbf{r}_\perp,z)$. In this equation the sum is carried over the layers indexed by n, ρ_s is the electron density of a single layer, d is the layer spacing, and $u_n(\mathbf{r}_\perp,t)$ is the averaged displacement of molecules situated around position $\mathbf{r}_\perp$ of layer number n. If random displacements u_n of the layers are Gaussian, then the intensity S in Eq. (2) is given by

$$\begin{aligned}S=|\rho_s(q_z)|^2\int d^2r_\perp\sum_{m,n}\exp\Big[&\imath(m-n)dq_z+\imath\mathbf{r}_\perp\cdot\mathbf{q}_\perp \\ &-\frac{1}{2}q_z^2 g_{mn}(\mathbf{r}_\perp,t)\Big],\end{aligned} \tag{4}$$

where

$$g_{mn}(\mathbf{r}_\perp,t)=\langle[u_m(0,0)-u_n(\mathbf{r}_\perp,t)]^2\rangle, \tag{5}$$

and $\rho_s(q_z)$ is the molecular form factor, the Fourier transform of the density $\rho_s(z)$. The indices m, n enumerate the smectic layers. Now all the dependence on time is in the displacement-displacement correlation function $g_{mn}(\mathbf{r}_\perp,t)$, which is central to the following considerations. The analysis of $g_{mn}(\mathbf{r}_\perp,t)$ carried out by Poniewierski *et al.* [2,3] is based on the following approach. First, they apply hydrodynamic equations for bulk smectic-A liquid crystals written in terms of a continuous displacement $u(\mathbf{r}_\perp,z,t)$. Second, they replace the derivative $\nabla_z u$ with $(u_n-u_{n-1})/d$, taking into ac-

count additional terms for the interfacial effects (surface tension), and obtain a set of coupled equations for the displacements $u_n(\mathbf{r}_\perp,t)$. In this paper we use the same hydrodynamic equations to calculate

$$g(\mathbf{r}_\perp,z,z',t)=\langle[u(0,z',0)-u(\mathbf{r}_\perp,z,t)]^2\rangle, \tag{6}$$

where z remains a continuous variable. In Eq. (4) we set

$$g_{mn}(\mathbf{r}_\perp,t)=g(\mathbf{r}_\perp,z_n,z_m,t), \tag{7}$$

where z_m and z_n are the z coordinates of smectic layers m and n, respectively.

III. Sm-*A* FILMS

A. Hydrodynamic equations of Sm-*A* films

The full set of hydrodynamic equations for a smectic-*A* liquid crystal can be found, for instance, in Refs. [14,16,18,19]. Here we use a simplified version. We first note that there are no fewer than three characteristic time scales for the hydrodynamics of smectic-*A* liquid crystals [16,20] (see also Ref. [21]). The first is the characteristic time of the permeation process, which can be viewed as penetration of flux through the smectic layer structure. This process is very weak and its characteristic time scale is very large. Second is the time required for viscous forces to respond to inertia. This motion is sometimes known in the literature as the fast mode [16], and its time scale is the shortest of the three. The final time scale comes from a balance between viscous and elastic forces. This is sometimes known in the literature as the slow mode, although its time scale is in fact intermediate. Due to the small parameter $\rho_0 K/\eta_3^2$ [16], which is of order 10^{-6}, one can consider separately the slow and fast modes in a bulk smectic liquid crystal. This parameter can be considered the ratio of inertia to elastic forces. The presence of this small parameter is due to the fact that a term proportional to $q_\perp^2$ is absent in the bulk elastic energy. Equations for the slow mode are obtained from the general hydrodynamic equations by neglecting inertial terms. One should be cautious in the case of a thin free-standing film, because this involves a surface contribution proportional to $q_\perp^2$ due to surface tension. If the layers undulate conformally, then this contribution operates effectively as a bulk one. For small $q_\perp$ this term prevails over the layer-bending term $Kq_\perp^4$ and the approximation based on neglecting inertia ceases to be valid. It is shown in Ref. [2] that this happens for $q_\perp^2<2\rho_0\gamma/\eta_3^2 L$, where L is the film thickness and γ is the surface tension. For typical parameters and two-layer films, this corresponds to $q_\perp<10^6\ \mathrm{m}^{-1}$, which is comparable to an experimental cutoff. The effect of the inertial term has been studied in Refs. [3] and [12] and also will be taken into account here in Sec. IV.

To outline our approach, in this section we will neglect the inertial terms and focus on only the slow mode, as in Ref. [2]. We also make the following assumptions. We neglect compressibility and take $\nabla\cdot\mathbf{v}=0$ while calculating viscous forces, where $\mathbf{v}$ is the velocity. In the time scale of the slow mode we neglect permeation, taking that $\mathbf{v}$ has only a z component with $v_z=\partial u/\partial t$. We also neglect rolls, and finally assume that temperature is constant ($\nabla T=0$).

In this approximation the viscous force is $\eta_3\nabla_\perp^2 v_z$ [16,18]. We recall that the free energy of a smectic-*A* liquid crystal film is [6,8,9]

$$F=\frac{1}{2}\int d^2r_\perp\left\{\int_{-L/2}^{L/2}dz\{B[\nabla_z u(\mathbf{r}_\perp,z)]^2+K[\nabla_\perp^2 u(\mathbf{r}_\perp,z)]^2\}+\gamma\{[\nabla_\perp u(\mathbf{r}_\perp,z=-L/2)]^2+[\nabla_\perp u(\mathbf{r}_\perp,z=L/2)]^2\}\right\}, \tag{8}$$

where B is the layer compression elastic constant. The boundaries of the film are at $z=\pm L/2$, where $L=Nd$ is the thickness of a film containing N layers. The elastic force is equal to the variational derivative

$$-\frac{\delta F}{\delta u}=-(-B\nabla_z^2+K\Delta_\perp^2)u. \tag{9}$$

The balance between the viscous and elastic forces yields

$$\eta_3\frac{\partial}{\partial t}\nabla_\perp^2 u-[-B\nabla_z^2+K\Delta_\perp^2]u=0. \tag{10}$$

Note that the discrete model [2] starts off with this equation. We shall apply the following boundary conditions:

$$-\frac{\gamma}{B}\nabla_\perp^2 u(\mathbf{r}_\perp,z=\pm L/2,t)\pm\nabla_z u(\mathbf{r}_\perp,z=\pm L/2,t)=0, \tag{11}$$

which are the the same as the static conditions obtained by minimizing F with respect to the surface displacements $u(\mathbf{r}_\perp,z=\pm L/2,t)$. Formally these boundary conditions mean that there is no viscosity and relaxation occurs instantaneously at the surfaces. Although these boundary conditions appear different from those used in the discrete model, they provide the same characteristic times of the relaxation modes. It is shown in the Appendix how these boundary conditions evolve into the ones used in Refs. [2,3]. The boundary conditions in Eq. (11) also are the same as those employed in Ref. [12].

B. Correlation function

According to Eq. (6) and (7), the correlation function $g_{mn}(\mathbf{r}_\perp,t)$ in Eq. (4) can be expressed as

$$g_{mn}(\mathbf{r}_\perp,t)=\frac{1}{(2\pi)^2}\int d^2q_\perp[G(\mathbf{q}_\perp,z_m,z_m,t)+G(\mathbf{q}_\perp,z_n,z_n,t)-2G(\mathbf{q}_\perp,z_n,z_m,t)\times\exp(\imath\mathbf{r}_\perp\cdot\mathbf{q}_\perp)], \tag{12}$$

where

$$G(\mathbf{q}_\perp,z,z',t)=\langle u^*(\mathbf{q}_\perp,z',0)u(\mathbf{q}_\perp,z,t)\rangle. \tag{13}$$

To calculate G we use the method developed in Ref. [6], which is based on the resolution function of the operator $-\nabla_z^2$. Mathematically this method is formulated as follows.

Taking the Fourier transform of Eq. (10) over the in-plane coordinates $\mathbf{r}_\perp$, multiplying by $u^*(\mathbf{q}_\perp,z',0)$, and averaging, we get the equation

$$\frac{\partial G(\mathbf{q}_\perp,z,z',t)}{\partial t}=-\frac{B}{\eta_3 q_\perp^2}\left[-\nabla_z^2+\frac{K}{B}q_\perp^4\right]G(\mathbf{q}_\perp,z,z',t), \tag{14}$$

with boundary conditions

$$\frac{\gamma q_\perp^2}{B}G(\mathbf{q}_\perp,z=\pm L/2,z',t)\pm\nabla_z G(\mathbf{q}_\perp,z=\pm L/2,z',t)=0, \tag{15}$$

which follow from Eq. (11), and the initial condition

$$G(\mathbf{q}_\perp,z,z',0)=G^0(\mathbf{q}_\perp,z,z'). \tag{16}$$

Here G^0 is the single-time correlation function found in Ref. [6] [see Eq. (24) below]. We will show in the Appendix that this formulation is equivalent to the discrete dynamical model developed in Refs. [2] and [3].

To solve these dynamical equations we will make the following transformation:

$$G^+(\mathbf{q}_\perp,z,z',\omega)=\int_0^\infty dt e^{\imath\omega t}G(\mathbf{q}_\perp,z,z',t). \tag{17}$$

Applying this to Eq. (14), integrating by parts and taking into account that the correlation function vanishes as $t\to\infty$, we obtain

$$[-\nabla_z^2-\lambda]G^+(\mathbf{q}_\perp,z,z',\omega)=\frac{\eta_3 q_\perp^2}{B}G^0(\mathbf{q}_\perp,z,z'), \tag{18}$$

where

$$\lambda(\mathbf{q}_\perp,\omega)=\imath\frac{\omega\eta_3 q_\perp^2}{B}-\frac{K}{B}q_\perp^4. \tag{19}$$

The solution to this equation can be expressed in terms of the resolution function

$$R_\lambda(z,z')=[-\nabla_z^2-\lambda]^{-1}(z,z'), \tag{20}$$

where the domain of the operator $-\nabla_z^2$ are functions satisfying the boundary conditions (11).

Here we will just present an expression for the resolution function (analytical details of the derivation can be found in Ref. [6]):

$$\begin{aligned}\tilde{R}_{\tilde{\lambda}}(\tilde{z},\tilde{z}')=&\frac{1}{2v[(v+w)^2-(v-w)^2e^{-2v}]}\{(v+w)^2e^{-v|\tilde{z}-\tilde{z}'|}\\&+2(v^2-w^2)^2e^{-v}\cosh(v|\tilde{z}+\tilde{z}'|)\\&+(v-w)^2e^{-2v+v|\tilde{z}-\tilde{z}'|}\},\end{aligned} \tag{21}$$

where v and w defined as

$$v=\sqrt{-\tilde{\lambda}},$$

$$w=\frac{\gamma\tilde{q}_\perp^2}{BL}, \tag{22}$$

where the tilde denotes dimensionless variables scaled with respect to L (for example, $\tilde{q}_\perp=Lq_\perp$, $\tilde{r}_\perp=r_\perp/L$, $\tilde{z}=z/L$), and $\tilde{R}$ is defined as

$$R_\lambda(z,z')=L\tilde{R}_{L^2\lambda}(z/L,z'/L). \tag{23}$$

Note that the single-time correlation function can be expressed in terms of the resolution function as [6]

$$G^0(\mathbf{q}_\perp,z,z')=\frac{k_BT}{B}R_{\lambda(\mathbf{q}_\perp,0)}(z,z'). \tag{24}$$

The solution to Eq. (18) is now given by

$$G^+(\mathbf{q}_\perp,z,z',\omega)=\frac{\eta_3 q_\perp^2 k_BT}{B^2}(R_{\lambda(\mathbf{q}_\perp,\omega)}\cdot R_{\lambda(\mathbf{q}_\perp,0)})(z,z'). \tag{25}$$

and the full correlation function is

$$G(\mathbf{q}_\perp,z,z',\omega)=G^+(\mathbf{q}_\perp,z,z',\omega)+G^+(\mathbf{q}_\perp,z,z',-\omega), \tag{26}$$

where we have used time-reversal symmetry. The product on the right-hand side of Eq. (25) can be calculated using the first formula for resolution functions of self-adjoint operators [22]

$$(R_\mu\cdot R_\nu)(z,z')=\frac{1}{\mu-\nu}[R_\mu(z,z')-R_\nu(z,z')]. \tag{27}$$

Then one finally obtains

$$G(\mathbf{q}_\perp,z,z',\omega)=\frac{2k_BT}{\omega B}\mathrm{Im}\,R_{\lambda(\mathbf{q}_\perp,\omega)}(z,z'). \tag{28}$$

The displacement-displacement correlation function in the real space and time representation is obtained from the Fourier transform

$$\begin{aligned}&\langle u(0,z',0)u(\mathbf{r}_\perp,z,t)\rangle\\&\quad=\frac{1}{(2\pi)^3}\int d\omega d^2q_\perp e^{-\imath\omega t+\imath\mathbf{q}_\perp\cdot\mathbf{r}_\perp}G(\mathbf{q}_\perp,z,z',\omega).\end{aligned} \tag{29}$$

The integration over $q_\perp$ is normally cut off in the short and long wavelength limits by the intermolecular distance a and in-plane size of the system Λ, respectively. However, for x-ray experiments the cutoff Λ is equal to the in-plane resolution length, which is normally much less than the in-plane size of the system [8,9]. It is also important to use a cutoff in the z direction [9], putting $|z-z'|=d/4$ for $m=n$, which accounts for layer smearing.

C. Eigenmodes and their characteristic times

The singularities of R as a complex function of ω have crucial physical significance. According to Eq. (20), the sin-

gularities of R correspond to values of $\lambda(\mathbf{q}_\perp,\omega)$ which are eigenvalues of the operator $-\nabla_z^2$. Since this operator with the given boundary conditions is self-adjoint, its eigenvalues must be real. Hence, according to Eq. (19), the frequencies ω corresponding to these singularities of R must be imaginary. From the definition (17), the function G^+ is regular in the region $\mathrm{Im}\,\omega>0$, and therefore each singular value of ω can be written as $-\imath/\tau$. Evaluating the Fourier transform over ω in Eq. (29), these singularities yield contributions with time dependence $\exp[-|t|/\tau]$, showing that the set of τ's are the relaxation times of the modes.

In a case of an infinite system one would obtain a continuous spectrum, with relaxation times $\tau(q_z)$ being continuous functions of wave number q_z in the z direction. Finiteness of the system in the z direction leads to quantization and as a result produces a discrete spectrum.

To calculate the characteristic times, one needs to find the roots of the denominator in Eq. (21). The denominator is zero if

$$\tanh(v)=-\frac{2vw}{v^2+w^2}. \tag{30}$$

Expressing $v=\imath wZ$, this becomes

$$\tan(wZ)=\frac{2Z}{Z^2-1}. \tag{31}$$

The singular values of v define via Eq. (22) the singular values of $\tilde{\lambda}$, which in turn define via Eq. (19) the corresponding singular values of ω. The characteristic times are therefore found to be

$$\tau_m=\frac{B\eta_3}{q_\perp^2[\gamma^2Z_m^2+KB]}, \tag{32}$$

where Z_m are the roots of Eq. (31), which will be ordered as $Z_1<Z_2<Z_3<\cdots$. For m odd (even), these correspond to symmetric (antisymmetric) modes [2,12,23].

Figure 1 illustrates the graphical solution of Eq. (31). The solid curve corresponds to $\tan(wZ)$ and is plotted for $w=0.5$. The intersections of the curves show the first three roots of Eq. (31).

The first root can be found easily for $w\ll 1$. It is useful to rewrite Eq. (31) as

$$(Z^2-1)\sin(wZ)-2Z\cos(wZ)=0. \tag{33}$$

Expanding this equation in powers of w,

$$-2+(Z_1^2-1)w+Z_1^2w^2-\frac{1}{6}(Z_1^2-1)Z_1^2w^3+O(w^4)=0, \tag{34}$$

leads to

$$Z_1^2\approx\frac{2}{w}-\frac{1}{3}=\frac{2B}{\gamma Lq_\perp^2}-\frac{1}{3}, \tag{35}$$

which in turn yields

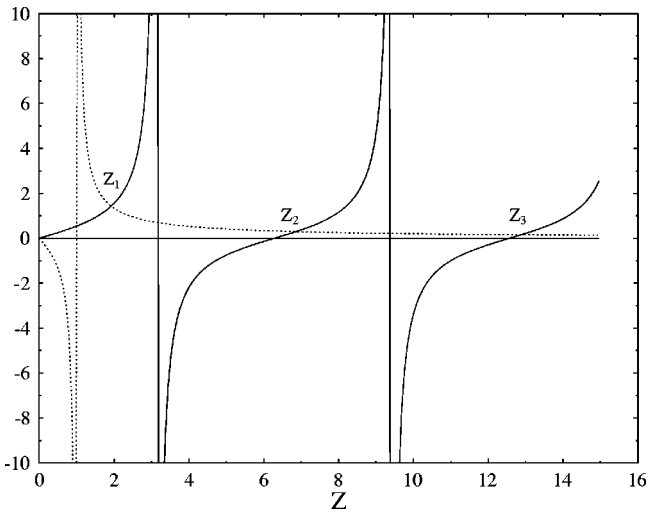

FIG. 1. The left- and right-hand sides of Eq. (31). The solid line corresponds to $\tan(wZ)$ and is plotted for $w=0.5$. It is seen that roots with large indices are close to zeros of $\tan(wZ)$.

$$\tau_1\approx\eta_3\left[\frac{2\gamma}{L}+\left(1-\frac{\gamma^2}{3KB}\right)Kq_\perp^2\right]^{-1}. \tag{36}$$

This expression is valid only for $q_\perp^2\ll B/\gamma L$. For $q_\perp=0$ this agrees with the result of Poniewierski *et al.* [2]:

$$\tau_1=\frac{\eta_3L}{2\gamma}. \tag{37}$$

Note that, in this range of $q_\perp$, τ_1 decreases with $q_\perp$ if $\gamma^2<3KB$ and increases if $\gamma^2>3KB$. A more detailed consideration (see also the results of numerical calculation below) shows that for $q_\perp=0$ only the first relaxation time is nonzero, while all the others vanish.

Note that the roots of Eq. (31) with large numbers m and nonzero w are approximately $Z_m=\pi m$. Therefore, for large m and $q_\perp\neq 0$ we have

$$\tau_m\approx\frac{B\eta_3}{q_\perp^2(\gamma^2\pi^2m^2+KB)}. \tag{38}$$

Figure 2 shows the first few characteristic times versus $q_\perp$. As noted above, only the first relaxation time τ_1 (denoted τ_0 in Refs. [2,3]) remains nonzero as $q_\perp\to 0$. The behavior of the relaxation times in Fig. 2 is identical to that obtained by more involved calculations in Ref. [2].

The correlation function $g_{mn}(\mathbf{r}_\perp,t)$, which determines the scattering intensity [see Eq. (4)], can be obtained by taking the inverse Fourier transform over ω and $\mathbf{q}_\perp$, see Eq. (29). We shall present results for $g_{mn}(\mathbf{r}_\perp,t)$ in the following section, after generalizing the theory to Cr-B films.

IV. Cr-B FILMS

A. Elastic energy of a hexagonal crystal

To account for the crystal structure of the Cr-B phase, it is instructive to consider deformations and the elastic energy associated with them. Deformations of 3D crystals are described by the strain tensor

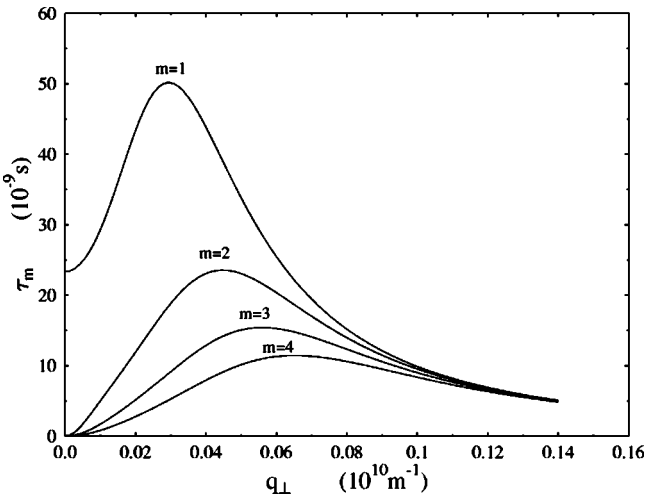

FIG. 2. Four relaxation times τ_m, $m=1,2,3,4$ vs in-plane wave number for a five-layer film with the parameters: $d=2.8\times10^{-9}$ m, $K=10^{-11}$ N, $B=2.5\times10^{6}$ N/m^2, $\gamma=3\times10^{-2}$ N/m, $\eta_3=0.1$ kg/s/m.

$$u_{ij}=\frac{1}{2}(\nabla_j u_i+\nabla_i u_j), \tag{39}$$

where **u** is the displacement vector. The elastic energy F for solids is quadratic in the symmetrized strains

$$F=\frac{1}{2}\int d^3r K_{ijlm}u_{ij}u_{lm}. \tag{40}$$

The elastic-constant tensor K_{ijlm} depends on the symmetry of the system. For a uniaxial system with symmetry axis along z we have [14,20]

$$\begin{aligned}F_{\text{uniaxial}}=\frac{1}{2}\int d^3r[&C_{11}(u_{xx}^2+u_{yy}^2)+2C_{12}u_{xx}u_{yy}\\&+2(C_{11}-C_{12})u_{xy}^2+C_{33}u_{zz}^2+C_{44}(u_{yz}^2+u_{xz}^2)\\&+2C_{13}(u_{xx}+u_{yy})u_{zz}].\end{aligned} \tag{41}$$

Here the elastic-constant tensor has the form

$$\begin{aligned}K_{ijlm}=&C_{33}a_ia_ja_la_m+\frac{1}{2}(C_{11}-C_{12})(\delta_{il}^{\perp}\delta_{jm}^{\perp}+\delta_{jl}^{\perp}\delta_{im}^{\perp})\\&+C_{12}\delta_{ij}^{\perp}\delta_{lm}^{\perp}+\frac{1}{4}C_{44}(a_ia_l\delta_{jm}^{\perp}+a_ja_l\delta_{im}^{\perp}+a_ia_m\delta_{jl}^{\perp}\\&+a_ja_m\delta_{il}^{\perp})+C_{13}(a_ia_j\delta_{lm}^{\perp}+a_la_m\delta_{ij}^{\perp}).\end{aligned} \tag{42}$$

In these equations, the quantity **a** takes its conventional meaning of a unit vector along the axis of symmetry, and

$$\delta_{ij}^{\perp}=\delta_{ij}-a_ia_j.$$

In our system of coordinates $a_i=\delta_{iz}$. The stress tensor can now be expressed as

$$\sigma_{ij}=\frac{\delta F}{\delta u_{ij}}=K_{ijlm}u_{lm}, \tag{43}$$

with K_{ijlm} given by Eq. (42).

A general approach to deriving dynamical equations of solids is formulated in Ref. [14]. For nondissipative systems, these equations describe a balance between elastic forces and inertia:

$$\rho_0\frac{\partial^2 u_i}{\partial t^2}=\nabla_j\sigma_{ij}. \tag{44}$$

If the system is viscous, σ_{ij} should be replaced by $\sigma_{ij}+\sigma_{ij}'$, where the tensor σ_{ij}' accounts for viscous forces and can be expressed through a dissipation function R as

$$\sigma_{ij}'=\frac{\delta R}{\delta v_{ij}}, \tag{45}$$

with

$$v_{ij}=\frac{\partial u_{ij}}{\partial t}. \tag{46}$$

The dissipation function R is quadratic in v_{ij}, has the same symmetry properties as the elastic energy, and can be written by analogy with Eq. (42) as

$$R=\frac{1}{2}\int d^3r\,\eta_{ijlm}v_{ij}v_{lm}, \tag{47}$$

with the viscosity tensor given by

$$\begin{aligned}\eta_{ijlm}=&\eta_1a_ia_ja_la_m+\eta_2(\delta_{il}^{\perp}\delta_{jm}^{\perp}+\delta_{jl}^{\perp}\delta_{im}^{\perp})+(\eta_4-\eta_2)\delta_{ij}^{\perp}\delta_{lm}^{\perp}\\&+\eta_3(a_ia_l\delta_{jm}^{\perp}+a_ja_l\delta_{im}^{\perp}+a_ia_m\delta_{jl}^{\perp}+a_ja_m\delta_{il}^{\perp})\\&+\eta_5(a_ia_j\delta_{lm}^{\perp}+a_la_m\delta_{ij}^{\perp}).\end{aligned} \tag{48}$$

The coefficients here are chosen to correspond to the form of the viscous tensor in a smectic liquid crystal. Note, however, that the values of the viscosity coefficients η_k can differ from those for a liquid smectic phase.

The dynamical equation accounting for the dissipative forces is now given by

$$\rho_0\frac{\partial^2 u_i}{\partial t^2}=\left[K_{ijlm}+\eta_{ijlm}\frac{\partial}{\partial t}\right]\nabla_j u_{lm}. \tag{49}$$

B. Easy-shear approximation

As seen from Eq. (49), in general there is a set of three coupled differential equations that characterize dynamics of small deformations of a crystal. Here we discuss a simplified version which, on one hand, is similar to the description of the Sm-*A* phase in Sec. III and, on the other hand, takes into account the crystalline structure of the Cr-*B* phase.

In fact, although the crystalline phase has a finite shear modulus C_{44}, it is abnormally small. The ratio C_{44}/C_{11} is reported to be 10^{-4} [24,25]. Since C_{44} is very small, the conventional analysis of bending [14], which ignores shear, is not valid. Here we consider the approximation where all in-plane deformations are neglected, while instead shear deformations are well developed, which is termed the easy-shear approximation. Mathematically, this approximation

corresponds to assuming that the displacement **u** can be expressed as

$$u_j(\mathbf{r}) = \delta_{jz} u(x,y,z). \tag{50}$$

The corresponding strain tensor elements are

$$u_{xz} = \frac{1}{2}\frac{\partial u}{\partial x}, \qquad u_{yz} = \frac{1}{2}\frac{\partial u}{\partial y}, \qquad u_{zz} = \frac{\partial u}{\partial z}, \qquad u_{xx} = u_{yy} = u_{xy} = 0. \tag{51}$$

Using these elements in Eq. (41), the latter becomes

$$F_{\text{uniax}} = \frac{1}{2}\int d^3r \left[C_{33}(\nabla_z u)^2 + \frac{1}{4} C_{44}(\nabla_\perp u)^2 \right]. \tag{52}$$

It is seen that C_{33} corresponds to the smectic compressibility coefficient B, and henceforth we will denote it as B instead of C_{33}, keeping in mind that its value can differ from that for a Sm-*A* phase. The shear elastic coefficient C_{44} is finite but small, so it is justified keeping the next-order term with respect to in-plane derivatives, which is a dominant term in the liquid smectic phase. Therefore, we end up with the elastic energy:

$$F = \frac{1}{2}\int d^3r \left[B(\nabla_z u)^2 + K(\Delta_\perp u)^2 + \frac{1}{4} C_{44}(\nabla_\perp u)^2 \right]. \tag{53}$$

A crucial consequence of shear elastic deformations is that they produce a bulk term proportional to $(\nabla_\perp u)^2$, which is forbidden in smectic phases where the layers slide freely. The absence of such a term leads to the Landau-Peierls instability of bulk smectic phases. Any finite C_{44} makes the mean-square fluctuations converge independently of the size of the system.

To use this approximation we should also include viscous forces. As we did earlier, we neglect compressibility by assuming $\nabla \cdot \mathbf{v} = 0$. The components v_x and v_y are equal to zero, due to Eq. (50). Hence, neglecting the compressibility, we also have $v_{zz} = 0$. Therefore, the only components giving contributions to the viscous forces are v_{zx} and v_{zy}. The dissipation function in terms of v_z is

$$R = \frac{1}{2}\int d^3r\, \eta_3 (\nabla_\perp v_z)^2. \tag{54}$$

The elastic and viscous forces acting in the z direction can be expressed as derivatives of F and R with respect to u and v_z, respectively. The dynamical equation (49) now reduces to [14]

$$\rho_0 \frac{\partial v_z}{\partial t} = -\frac{\delta F}{\delta u} - \frac{\delta R}{\delta v_z}. \tag{55}$$

Using Eqs. (53) and (54), this becomes

$$\rho_0 \frac{\partial^2 u(\mathbf{r},t)}{\partial t^2} = \left[\eta_3 \frac{\partial}{\partial t}\Delta_\perp + B\nabla_z^2 + \frac{1}{4} C_{44}\Delta_\perp - K\Delta_\perp^2 \right] u(\mathbf{r},t). \tag{56}$$

Taking the Fourier transform over $\mathbf{r}_\perp$, we get

$$\rho_0 \frac{\partial^2 u(\mathbf{q}_\perp, z, t)}{\partial t^2} = \left[-\eta_3 q_\perp^2 \frac{\partial}{\partial t} + B\nabla_z^2 - \frac{1}{4} C_{44} q_\perp^2 - K q_\perp^4 \right] u(\mathbf{q}_\perp, z, t). \tag{57}$$

As shown in Refs. [2,3] (see also Refs. [21,26] for discussion of the characteristic times), the inertial term in the case of a smectic phase is usually negligible on the time scales of interest. To check the validity of this approximation in the present case, we first estimate the characteristic time provided by the balance of viscous and elastic forces:

$$\tau = \eta_3 \left[\frac{1}{4} C_{44} + K q_\perp^2 \right]^{-1}. \tag{58}$$

The ratio of inertia to the elastic force is then given by

$$\frac{\rho_0 K}{\eta_3^2} \left(1 + \frac{C_{44}}{4K q_\perp^2} \right)^2. \tag{59}$$

We recall that the prefactor $\rho_0 K/\eta_3^2$ is a small parameter of order $10^{-6}-10^{-5}$. Therefore the inertial term is negligible when the following criterion is satisfied:

$$\frac{\rho_0 C_{44}^2}{16 K \eta_3^2 q_\perp^4} \ll 1. \tag{60}$$

Taking $C_{44} = 10^5$ N/m^2, $K = 10^{-11}$ N, $\eta_3 = 10^{-1}$ kg/m/s, $\rho_0 = 10^3$ kg/m^3, Eq. (60) gives $q_\perp \gg 1.6 \times 10^6$ m^{-1}. Hence, for smaller $q_\perp$ one has to keep the inertial term in the dynamical equation, which means that the slow and fast modes cannot be considered separately for such small values of $q_\perp$. In the following we derive the displacement-displacement correlation function taking into account the inertial term. We recall that, for very thin smectic films fluctuating conformally, the inertial term is not negligible due to the surface tension, as mentioned in Ref. [2]. This is also true in the case of the Cr-*B* film. The criterion (60) does not involve the film thickness and thus provides a further reason for taking the inertial term into account.

C. Correlation function for a Cr-*B* film

The displacement-displacement correlation function is the solution to the equation

$$\rho_0 \frac{\partial^2 G(\mathbf{q}_\perp, z, z', t)}{\partial t^2} = -\eta_3 q_\perp^2 \frac{\partial G(\mathbf{q}_\perp, z, z', t)}{\partial t} - B\left[-\nabla_z^2 + \frac{C_{44}}{4B} q_\perp^2 + \frac{K}{B} q_\perp^4\right] G(\mathbf{q}_\perp, z, z', t), \tag{61}$$

with the same boundary conditions as in Eq. (15) and initial condition (16) as well as

$$\frac{\partial}{\partial t} G(\mathbf{q}_\perp, z, z', t=0) = 0. \tag{62}$$

The latter initial condition follows from the fact that u and v_z are statistically independent (see also Ref. [3]).

To solve this dynamical equation we make the the same transformation as in the case of Sm-*A* films in Eq. (17). Integrating by parts leads to the equation

$$[-\nabla_z^2 - \lambda] G^+(\mathbf{q}_\perp, z, \omega) = \left(\frac{\eta_3 q_\perp^2}{B} - \frac{\imath \rho_0 \omega}{B}\right) G^0(\mathbf{q}_\perp, z, z'), \tag{63}$$

where λ is now given by

$$\lambda(\mathbf{q}_\perp, \omega) = \imath \frac{\omega \eta_3 q_\perp^2}{B} + \frac{\rho_0 \omega^2}{B} - \frac{C_{44}}{4B} q_\perp^2 - \frac{K}{B} q_\perp^4. \tag{64}$$

For $\rho_0 = 0$ and $C_{44} = 0$ this is identical to the corresponding expression (19) for the slow mode in a Sm-*A* film. The solution of Eq. (63) is the same as for Eq. (18), differing only in the expressions on the right-hand side and for λ. Repeating the same arguments as in Sec. III we obtain the same final expression (28) for G, but with λ defined by Eq. (64).

D. Eigenmodes of the Cr-*B* film and their characteristic times

To analyze the relaxation times we again consider the zero points of the dominator in Eq. (21). As in the case of a smectic film, we set $\omega = -\imath/\tau$, $v = \imath w Z$. The relaxation times are now the roots of the equation

$$\rho_0 \frac{1}{\tau^2} - \eta_3 q_\perp^2 \frac{1}{\tau} + \frac{1}{4} C_{44} q_\perp^2 + K q_\perp^4 + \frac{\gamma^2 q_\perp^4}{B} Z_m^2 = 0. \tag{65}$$

Hence, for any Z_m we now have two characteristic times. The larger one corresponds to the slow mode in the Sm-*A* phase. The other one corresponds to the fast mode, which we did not consider in Sec. III. For $m = 1$ and small $q_\perp$ we again can use Eq. (35). This yields the approximation

$$\rho_0 \frac{1}{\tau_1^2} - \eta_3 q_\perp^2 \frac{1}{\tau_1} + K\left(1 - \frac{\gamma^2}{3KB}\right) q_\perp^4 + \left(\frac{2\gamma}{L} + \frac{1}{4} C_{44}\right) q_\perp^2 = 0. \tag{66}$$

Expanding the roots of Eq. (66) in powers of $q_\perp$, we obtain

$$\frac{1}{\tau_1} \approx \mp \imath \frac{1}{2} \sqrt{\frac{L C_{44} + 8\gamma}{\rho_0 L}} q_\perp + \frac{\eta_3}{2\rho_0} q_\perp^2. \tag{67}$$

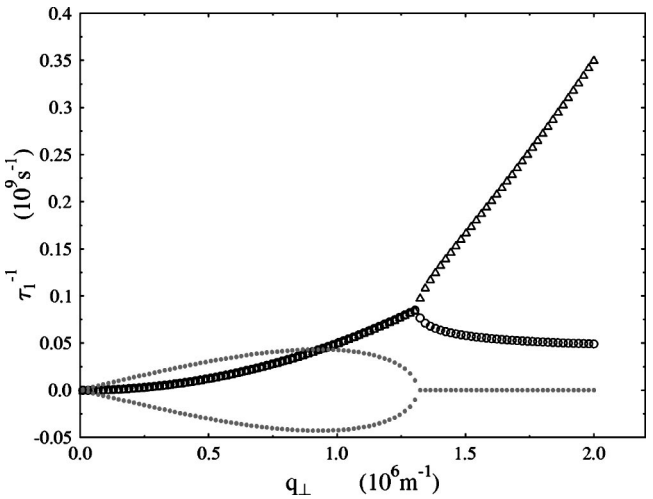

FIG. 3. The first inverse relaxation time τ_1^{-1} vs in-plane wave number $q_\perp$. The triangles and circles show the real part of the fast and slow branches, respectively. The dots show the imaginary part of the first relaxation time of both of the branches. These results are for a five-layer film with the parameters $K = 10^{-11}$ N, $B = 2.5 \times 10^6$ N/m^2, $\gamma = 3.0 \times 10^{-2}$ N/m, $\eta_3 = 0.1$ kg/s/m, $C_{44} = 10^5$ N/m^2, $d = 2.8 \times 10^{-9}$ m, $\rho_0 = 10^3$ kg/m^3.

Figures 3 and 4 show the inverse relaxation times of the slow and fast branches of the first two modes due to Z_1 and Z_2, respectively. The values of Z_1 and Z_2 have been found numerically by solving Eq. (31). Both real and imaginary parts of the relaxation times are shown. The curves in Fig. 3 confirm the behavior of the real and and imaginary parts predicted by Eq. (67) in the region of small $q_\perp$. In contrast to the analysis in Sec. III, the relaxation times do not remain finite as $q_\perp$ vanishes, but diverge to infinity (see also Refs. [3,12]).

The correlation function $g_{mn}(\mathbf{r}_\perp, t)$, which is relevant to x-ray scattering, can be obtained by taking the inverse Fourier transforms, see Eqs. (29) and (12). Figure 5 shows re-

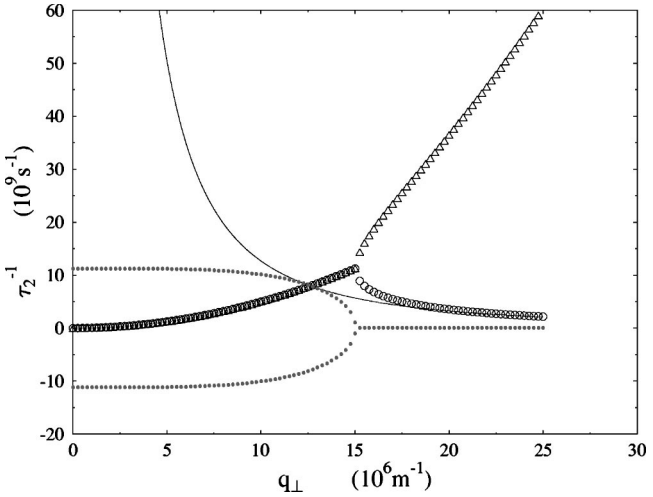

FIG. 4. The second inverse relaxation time τ_2^{-1} vs in-plane wave number $q_\perp$. The triangles and circles show the real part of the fast and slow branches, respectively. The dots show the imaginary part of the second relaxation time, producing oscillations in the correlation functions. The solid line shows the second inverse relaxation time worked out using Eq. (32) for a smectic film. All parameters are the same as for Fig. 3.

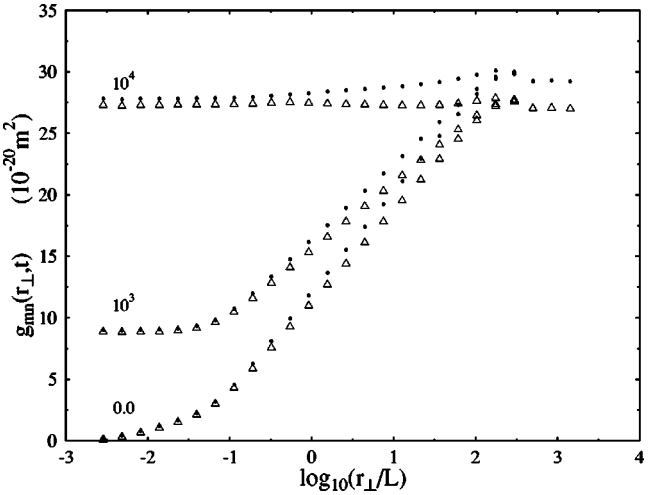

FIG. 5. The two-time displacement-displacement correlation function $g_{mn}(r_\perp,t)$ vs in-plane distance $r_\perp$ at various times $(B/\eta_3)t=0,10^3,10^4$, for a 50-layer Sm-*A* (dots) and Cr-*B* (triangles) film with $m=n=25$, $C_{44}=10^5$ N/m^2, and $\rho_0=10^3$ kg/m^3. The following parameters are taken to be the same for the Sm-*A* and Cr-*B* phases: $B=10^9$ N/m^2, $K=10^{-11}$ N, $\gamma=2\times10^{-2}$ N/m, $\eta_3=0.1$ kg/s/m, $d=2.8\times10^{-9}$ m, $k_BT=4.45\times10^{-21}$ J. The short and long wavelength cutoffs are taken to be $a=4\times10^{-10}$ m and $\Lambda=2\times10^{-4}$ m, respectively.

sults of numerical calculations carried out for various reduced times $(B/\eta_3)t=0,10^3,10^4$ for a 50-layer Sm-*A* (dots) and Cr-*B* (triangles) film with $m=n=25$. The values of other parameters used are indicated in the figure caption. Small bumps in the curves in a narrow region around $r_\perp=\Lambda$ are due to the cutoff of the integration in the long-wavelength limit. Figure 5 shows negligible differences between the correlation functions for the Sm-*A* and Cr-*B* films at short in-plane distances. Significant differences occur at large in-plane distances, i.e., in the long wavelength limit. These differences are primarily due to C_{44} rather than inertial effects contributed by ρ_0, since the latter do not affect the final state. Note the approximately linear dependence of both the Sm-*A* and Cr-*B* correlation functions on $\log(r_\perp)$ before the cutoff takes effect, agreeing with the analyses in Refs. [3,12].

E. High compressibility approximation

In the case of thin films that undulate conformally we can neglect layer compressibility and assume *B* to be infinitely large. In this limit the correlation function *G* does not depend on *z* and z' and the film can be considered as a 2D system. Taking the limit $B\to\infty$ in Eq. (28), one obtains

$$G(\mathbf{q}_\perp,\omega)=\frac{2k_BT}{L\omega}\mathrm{Im}\left[\left(\frac{2\gamma}{L}+\frac{1}{4}C_{44}\right)q_\perp^2+Kq_\perp^4-\rho_0\omega^2-\imath\omega\eta_3q_\perp^2\right]^{-1}. \tag{68}$$

Again, the singular points of this function define the characteristic times. Expressing $\omega=-\imath/\tau$, we obtain the equation

$$\rho_0\frac{1}{\tau^2}-\eta_3q_\perp^2\frac{1}{\tau}+Kq_\perp^4+\left(\frac{2\gamma}{L}+\frac{1}{4}C_{44}\right)q_\perp^2=0, \tag{69}$$

which resembles the more exact equation (66) due to Z_1. Note that Eq. (69) yields the same relaxation time for small $q_\perp$ given by Eq. (67). Suppose the roots are denoted τ_s and τ_f, where *s* and *f* stand for slow and fast. Note also that the real parts of the roots of Eq. (69) are always positive and their imaginary parts are always opposite to each other. To simplify calculating the Fourier transform over ω, it is useful to rewrite Eq. (68) as

$$G(\mathbf{q}_\perp,\omega)=\frac{2k_BT(\tau_s+\tau_f)}{L\rho_0\tau_s\tau_f(\omega+\imath/\tau_s)(\omega-\imath/\tau_s^*)(\omega+\imath/\tau_f)(\omega-\imath/\tau_f^*)}. \tag{70}$$

Fourier transformation yields

$$G(\mathbf{q}_\perp,t)=\frac{1}{2\pi}\int_{-\infty}^{\infty}d\omega e^{-\imath\omega t}G(\mathbf{q}_\perp,\omega)=\frac{2k_BT(\tau_s+\tau_f)\tau_s\tau_f}{L\rho_0}\left[\frac{\tau_s^2}{(\tau_s+\tau_s^*)(\tau_s+\tau_f^*)(\tau_s-\tau_f)}\times e^{-|t|/\tau_s}+\frac{\tau_f^2}{(\tau_f+\tau_f^*)(\tau_f+\tau_s^*)(\tau_f-\tau_s)}e^{-|t|/\tau_f}\right]. \tag{71}$$

The relaxation times τ_s and τ_f depend on the wave number $q_\perp$. For sufficiently large $q_\perp$ both relaxation times are real. When $\tau_s\gg\tau_f$, i.e., in the limit of very large $q_\perp$, Eq. (71) describes relaxation with the single characteristic time τ_s. If

$$q_\perp^2<q_c^2\equiv\rho_0\left(\frac{8\gamma}{L}+C_{44}\right)(\eta_3^2-4\rho_0K)^{-1}, \tag{72}$$

then the roots of Eq. (69) are complex. For the same set of parameters as used for Fig. 3 this criterion yields $q_\perp<1.3\times10^6\mathrm{m}^{-1}$, which fits the results of numerical calculation shown in Fig. 3. In this range of $q_\perp$ the roots of Eq. (69) can be written as $\tau_{s,f}=\tau'\pm\imath\tau''$ with real and positive values of τ', τ''. The value $(\tau'^2+\tau''^2)/\tau'$ is the characteristic time for exponential decay, while $\tau''/(\tau'^2+\tau''^2)$ is the frequency of oscillations.

To show how this can affect x-ray scattering data, we calculate the time-dependent part S^2 of the intensity. To model a real experiment, we will incorporate into Eq. (4) an instrumental resolution function used in rocking geometry. In this geometry one of the detector slits is wide open, while the other remains narrow with inverse width Δq_x. In this case the 2D integral in Eq. (4) is reduced to an integral over *x* with the weight function $\exp[-(x\Delta q_x)^2/2]$. The details as well as general consideration of the effects of an instrumental resolution function on the data in an arbitrary geometry can be found in Ref. [27]. We recall that for a thin uniformly

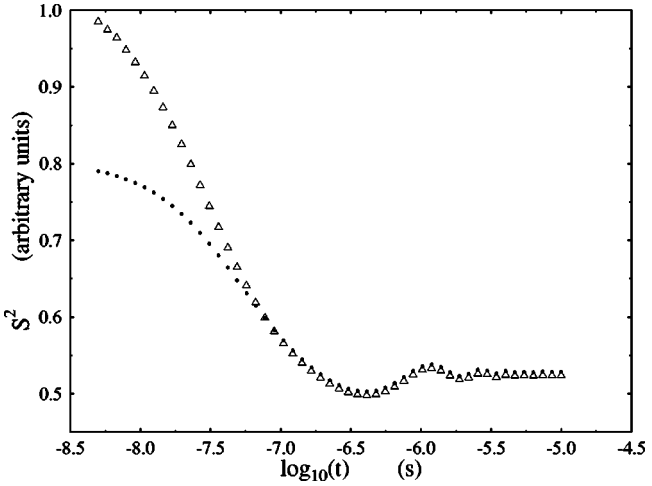

FIG. 6. The time-dependent part $|S|^2$ of the two-time intensity-intensity correlation function with an instrumental resolution function used in rocking geometry. The calculations have been carried out for a five-layer Cr-*B* film using Eqs. (71), (73), and (74). The components of the scattering vector are $\mathbf{q}_\perp=0$, $q_z=2\pi/d$ and the inverse instrumental resolution length are $\Delta q_x=10^6$ m^{-1} (dots), $\Delta q_x=10^7$ m^{-1} (triangles). The cutoffs are the same as for Fig. 5, while all other parameters are the same as for Fig. 3.

undulating film the displacement-displacement correlation function is independent of the layer numbers m and n. Therefore, Eq. (4) becomes

$$S\propto\int_{-\infty}^{\infty}dx\exp\left[\imath q_x x-\frac{1}{2}(\Delta q_x x)^2-\frac{1}{2}q_z^2 g(x,t)\right], \quad (73)$$

where the correlation function g is calculated from

$$g(r_\perp,t)=\frac{1}{\pi}\int_{2\pi/\Lambda}^{2\pi/a}dq_\perp q_\perp[G(q_\perp,0)-J_0(r_\perp q_\perp)G(q_\perp,t)], \quad (74)$$

J_0 denoting the zeroth-order Bessel function.

Equations (71), (73), and (74) allow one to calculate the intensity-intensity correlation function measured in coherent x-ray experiments. Figure 6 shows the intensity-intensity correlation function for a five-layer Cr-*B* film at the Bragg peak ($q_\perp=0$, $q_z=2\pi/d$). The instrumental cutoff $\Delta q_x=10^6$ m^{-1} corresponds to a real experiment [9]. One can clearly see oscillatory behavior that stems from nonoverdamped fluctuations with wave numbers $q_\perp<q_c$. These oscillations result primarily from inertial effects due to surface tension rather than shear effects. In fact, essentially identical results are obtained for a Sm-*A* film in this thin-film regime, since the C_{44} term in Eqs. (68), (69), and (72) is negligible compared with the γ/L term in those equations, for small thickness L. Thus oscillations in g should be observable for both Sm-*A* and Cr-*B* films which are sufficiently thin, as has been indicated by preliminary experiments [28].

V. DISCUSSION AND CONCLUSIONS

In this paper, we have developed a continuous dynamical model which allows one to calculate the two-time density-density correlation function for Sm-*A* as well as Cr-*B* films, taking into account finite-size effects and surface tension. In the case of Sm-*A* free-standing films, the model is identical to that discussed in Ref. [12]. Here we show how the relaxation times of the system result from poles of the resolution function, written explicitly in Eq. (21). The model yields the same relaxation times as the discrete model [2,3], but using a considerably simpler analysis. As an example of the advantages of the continuous model, Eq. (36) predicts the growth of the first relaxation time with $q_\perp$ if $\gamma^2>3KB$, and decrease in the opposite case, for small $q_\perp$. This theoretical result is difficult to achieve via numerical calculations based on the discrete model. In the limiting case $q_\perp=0$, Eq. (36) provides the same behavior of the relaxation time as measured by Price *et al.* [1].

To the best of our knowledge, this is the first time that the dynamic correlation function has been discussed in the case of Cr-*B* films. We have been shown that although the Cr-*B* phase has a true 3D ordering, its fluctuations resemble random undulations of layers in the Sm-*A* phase. This occurs due to an abnormally small shear elastic constant. The positional order does not give rise to a large bending rigidity caused by compression and stretching of the top and bottom layers, since the stresses are quenched by well-developed shear deformations. We have developed the easy-shear approximation, which allows us to distinguish the main features of the system using an analysis which retains the simplicity of that applied to Sm-*A* films. It has been shown that the shear elasticity affects the relaxation times in the long wavelength limit. In this limit the inertial term in the dynamical equations is important and one has to consider the slow and fast modes together. This has several effects on the relaxation times. First, the relaxation times are complex in the long wavelength limit. The real parts correspond to relaxation, while the imaginary parts produce oscillations in the correlation functions. Second, all real parts of the relaxation times diverge as $q_\perp\to0$, in contrast to the results for smectic-*A* films obtained on neglecting the fast mode. Third, in the range where the relaxation times are complex, the real parts of the slow and fast modes are equal to each other, while their imaginary parts are opposite to each other. This has an important consequence for x-ray scattering because the density-density correlation is mainly driven by long wavelength undulations of the layers. Figure 6 shows that the nonmonotonic behavior of the intensity-intensity correlation function, which stems from the long wavelength undulations, is present even if the long wavelength range is ''screened'' by the instrumental resolution length ($q_c<\Delta q_x$).

Although we have concentrated on applications to coherent x-ray scattering, the two-time displacement-displacement correlation functions for the Sm-*A* and Cr-*B* phases derived in this paper can also be used for calculating the intensity-intensity correlation function in conventional dynamic light-scattering experiments. Both Sm-*A* and Cr-*B* phases are optically anisotropic. Random undulations of the layers lead to fluctuations of the director, which scatters light. A detailed analysis of the finite-size and surface effects on static light scattering can be found in Ref. [6]). In the case of dynamic light-scattering we need the displacement-displacement correlation function either in the $(\mathbf{q}_\perp,z,z',t)$ or $(\mathbf{q}_\perp,z,z',\omega)$ representations, rather than in the $(\mathbf{r}_\perp,z,z',t)$ representation. This significantly simplifies the analysis. Another simplifica-

tion arises from the fact that films of a few hundred layers can be considered incompressible, because light is not able to probe the layer spacing distance. Therefore, one can use the explicit formula (71) to evaluate the scattering intensity.

ACKNOWLEDGMENTS

This study was supported by the Natural Sciences and Engineering Research Council (Canada). A.S. also appreciates the hospitality of the Institute for Atomic and Molecular Physics (Amsterdam, the Netherlands) and thanks W.H. de Jeu and B. Ostrovskii for many fruitful discussions.

APPENDIX: EQUIVALENCE TO THE DISCRETE MODEL

In this appendix we show the equivalence of the discrete model [2,3] and the continuous model developed in this paper. The continuous model is specified by the equation [see Eq. (10)]

$$\frac{\eta_3 q_\perp^2}{B}\frac{\partial u(q_\perp,z,t)}{\partial t}=-\left[-\nabla_z^2+\frac{K}{B}q_\perp^4\right]u(q_\perp,z,t), \quad \text{(A1)}$$

with z varying from $-L/2$ to $L/2$, as well as by the boundary conditions (11). Let us try to solve this equation using the following approximation. The range $[-L/2,L/2]$ is split into $M+1$ sections of width $h=L/(M+1)$. The boundaries of these sections are $-L/2$, $-L/2+h$, $-L/2+2h$, ... The corresponding values of u are denoted $u_0=u(z=-L/2)$, $u_1=u(z=-L/2+h)$, . . . , $u_{M+1}=u(z=L/2)$. The solution to the differential equation (A1) is approximated by the solution to the following set of difference equations

$$\frac{\eta_3 q_\perp^2}{B}\frac{\partial u_j}{\partial t}=\frac{1}{h^2}(u_{j+1}-2u_j+u_{j-1})-\frac{K}{B}q_\perp^4 u_j, \quad \text{(A2)}$$

for $j=1 \ldots M$, together with the boundary conditions

$$\frac{\gamma q_\perp^2}{B}u_M+\frac{1}{h}(u_{M+1}-u_M)=0,$$

$$\frac{\gamma q_\perp^2}{B}u_1-\frac{1}{h}(u_1-u_0)=0. \quad \text{(A3)}$$

From Eq. (A3) we can express u_0 and u_{M+1} as

$$u_0=\left(1-\frac{\gamma q_\perp^2}{B}h\right)u_1, \quad \text{(A4)}$$

$$u_{M+1}=\left(1-\frac{\gamma q_\perp^2}{B}h\right)u_M, \quad \text{(A5)}$$

and substitute them into Eq. (A2). This leads to

$$\frac{\eta_3 q_\perp^2}{B}\frac{\partial u_1}{\partial t}=\frac{1}{h^2}(u_2-u_1)-\left(\frac{K}{B}q_\perp^4+\frac{\gamma q_\perp^2}{Bh}\right)u_1,$$

$$\frac{\eta_3 q_\perp^2}{B}\frac{\partial u_M}{\partial t}=\frac{1}{h^2}(-u_M+u_{M-1})-\left(\frac{K}{B}q_\perp^4+\frac{\gamma q_\perp^2}{Bh}\right)u_M. \quad \text{(A6)}$$

The other equations are the same as in Eq. (A2). If we take M to be the number of smectic layers and h to be the layer spacing d, then this set of equations coincides with that used in the discrete model [2].

[1] A. C. Price, L. B. Sorensen, S. D. Kevan, J. Toner, A. Poniewierski, and R. Holyst, Phys. Rev. Lett. **82**, 755 (1999).

[2] A. Poniewierski, R. Holyst, A. C. Price, L. B. Sorensen, S. D. Kevan, and J. Toner, Phys. Rev. E **58**, 2027 (1998).

[3] A. Poniewierski, R. Holyst, A. C. Price, and L. B. Sorensen, Phys. Rev. E **59**, 3048 (1999).

[4] A. Bottger and J. H. Joosten, Europhys. Lett. **4**, 1297 (1987).

[5] S. Sprunt, M. S. Spector, and J. Litster, Phys. Rev. A **45**, 7355 (1992).

[6] A. N. Shalaginov and V. P. Romanov, Phys. Rev. E **48**, 1073 (1993).

[7] R. Holyst, Phys. Rev. A **42**, 7511 (1990).

[8] R. Holyst, Phys. Rev. A **44**, 3692 (1991).

[9] E. A. L. Mol, J. D. Shindler, A. N. Shalaginov, and W. H. de Jeu, Phys. Rev. E **54**, 536 (1996).

[10] J. D. Shindler, E. A. L. Mol, A. N. Shalaginov, and W. H. de Jeu, Phys. Rev. Lett. **74**, 722 (1995).

[11] A. Fera *et al.*, Phys. Rev. E **60**, R5033 (1999).

[12] H. Y. Chen and D. Jasnow, Phys. Rev. E **61**, 493 (2000).

[13] A. Fera, R. Opitz, B. I. Ostrovskii, and W. H. de Jeu (unpublished).

[14] L. D. Landau and E. M. Lifshitz, *Theory of Elasticity* (Pergamon, Oxford, 1986).

[15] C. Zakri *et al.*, Phys. Rev. B **55**, 14 163 (1997).

[16] P. G. de Gennes and J. Prost, *The Physics of Liquid Crystals* (Clarendon, Oxford, 1993).

[17] G. F. Mazenko, S. Ramaswamy, and J. Toner, Phys. Rev. A **28**, 1618 (1983).

[18] P. C. Martin, O. Parodi, and P. S. Pershan, Phys. Rev. B **6**, 2401 (1972).

[19] E. I. Kats and V. V. Lebedev, *Dynamics of Liquid Crystals* (Springer, Berlin, 1993).

[20] P. M. Chaikin and T. C. Lubensly, *Principles of Condensed Matter Physics* (Cambridge University Press, Cambridge, 1995).

[21] A. N. Shalaginov, L. D. Hazelwood, and T. J. Sluckin, Phys. Rev. E **58**, 7455 (1998).

[22] M. Reed and B. Simon, *Methods of Modern Mathematical Physics* (Academic Press, Cambridge, 1972), Vol. 2.

[23] Equation (31) can be expressed as $Z=\pm[\cot(wZ/2)]^{\pm 1}$, which is identical to the relation for the roots in Ref. [12] for the symmetric $(+)$ and antisymmetric $(-)$ modes, respectively.

[24] M. Cagnon and G. Durand, Phys. Rev. Lett. **45**, 1418 (1980).

[25] E. Dubois-Violette, B. Pansu, P. Davidson, and A. M. Levelut, J. Phys. II **3**, 395 (1993).
[26] A. N. Shalaginov, L. D. Hazelwood, and T. J. Sluckin, Phys. Rev. E **60**, 4199 (1999).
[27] D. Sentenac, A. N. Shalaginov, A. Fera, and W. H. de Jeu, J. Appl. Crystallogr. **33**, 130 (2000).
[28] A. Fera, R. Opitz, I. Dolbnya, G. Gruebel, B. I. Ostrovskii, and W. H. de Jeu (unpublished).